Agricultural and Forest Meteorology 284 (2020) 107905

Contents lists available at ScienceDirect

Agricultural and Forest Meteorology

journal homepage: www.elsevier.com/locate/agrformet

Modification of surface energy balance during springtime: The relative importance of biophysical and meteorological changes

Minkyu Moon[a,*], Dan Li[a], Weilin Liao[b], Angela J. Rigden[c], Mark A. Friedl[a]

[a] Department of Earth and Environment, Boston University, Boston, MA, United States
[b] School of Geography and Planning, Sun Yat-sen University, Guangzhou, China
[c] Department of Earth and Planetary Sciences, Harvard University, Cambridge, MA, United States

ARTICLE INFO

Keywords:
Spring phenology
Aerodynamic resistance
Surface resistance
Bowen ratio
Specific humidity
Wind speed

ABSTRACT

In ecosystems characterized by strong seasonality in leaf area, the emergence of leaves during springtime modifies land surface energy balance by altering surface biophysical properties during a period when atmospheric conditions are also changing. However, the relative importance and interactions among surface biophysical and atmospheric variables in modifying the surface energy balance are not well understood. In this study, we use a physically-based attribution method to quantify the relative importance of covarying surface biophysical and atmospheric variables in modifying the surface energy balance during springtime. Results show that the widely observed decrease in the Bowen ratio that occurs with leaf emergence is not solely attributable to the sharp decrease in surface resistance caused by increasing leaf area. Rather, decreases in the Bowen ratio reflect the combined effects of changes in surface properties and atmospheric conditions. Specifically, decreasing surface resistance and increasing air temperature both act to reduce the Bowen ratio, while concurrent increases in specific humidity provide a negative feedback that constrains evaporative fluxes. In parallel, aerodynamic resistance tends to increase after leaf emergence largely because wind speed tends to decrease during springtime. These findings provide a refined characterization of surface energy balance dynamics during springtime when both surface and atmospheric conditions are changing rapidly and reveal previously understudied properties of the near-surface atmosphere that influence surface Bowen ratio and aerodynamic resistance.

1. Introduction

It has long been known that vegetation influences weather and climate (Sellers et al., 1997) and that phenology plays an important role in regulating interactions between the land surface and the atmosphere (Richardson et al., 2013). Specifically, vegetation phenology regulates seasonal variations in mass and energy exchange between terrestrial ecosystems and the atmosphere by modifying surface biophysical properties and processes including land surface albedo (Moore et al., 1996; Ollinger et al., 2008), aerodynamic and surface resistances (Blanken and Black, 2004; Zhao et al., 2016), and the partitioning of available energy into latent and sensible heat fluxes (Hogg et al., 2000; Schwartz, 1992). At the same time, vegetation phenology also affects a number of atmospheric properties and processes including daily air temperature range (Schwartz, 1996), cloud formation (Freedman et al., 2001), and precipitation (Zhang et al., 2005). Therefore, understanding the role of vegetation phenology in land-atmosphere interactions is essential to improving weather and climate models, and to understanding how ecosystems will respond to and affect future climate change (Peñuelas et al., 2009; Pielke et al., 1998; Richardson et al., 2013; Wilson and Baldocchi, 2000).

Changes in the surface energy balance during phenological transition periods have been previously documented (e.g., Fitzjarrald et al., 2001; Moore et al., 1996; Pielke et al., 1998; Ryu et al., 2008; Schwartz and Crawford, 2001; Wilson and Baldocchi, 2000). However, most of these previous studies are empirical, and none provide a physically-based framework for quantifying how the independent and joint contributions of changes in surface biophysical and meteorological properties influence changes in surface energy balance. Development of such a framework is challenging because vegetation phenology modulates a number of biophysical properties and meteorological processes concurrently. In particular, increased available energy from solar radiation during springtime causes air temperatures to increase, which triggers leaf emergence (Chuine et al., 2013; Friedl et al., 2014). At the same time, higher evaporative demand and canopy conductance from leaves in the vegetation canopy lead to greater partitioning of available

* Corresponding author.
E-mail address: mkmoon@bu.edu (M. Moon).

https://doi.org/10.1016/j.agrformet.2020.107905
Received 19 June 2019; Received in revised form 2 January 2020; Accepted 12 January 2020
0168-1923/ © 2020 Elsevier B.V. All rights reserved.

energy into evaporative fluxes (Monteith and Unsworth, 2013). Changes in surface albedo and roughness associated with leaf emergence introduce additional complexity. For example, increasing (decreasing) albedo will decrease (increase) available energy by reflecting (absorbing) more solar radiation from the surface, while an increase in the roughness length will enable more efficient transfer of sensible and latent heat from the surface to the atmosphere (Bonan, 2008).

Energy balance-based approaches have been widely used to study how the surface energy balance is modified by land use and land cover change (e.g., deforestation and urbanization; Chen and Dirmeyer, 2016; Devaraju et al., 2018; Lee et al., 2011; Li et al., 2019; Liao et al., 2018; Luyssaert et al., 2014; Zhao et al., 2014). Notably, the Intrinsic Biophysical Mechanism (IBM) method proposed by Lee et al. (2011) has been used to separate surface biophysical effects into three components: radiative forcing, aerodynamic resistance, and partitioning of available energy between latent and sensible heat fluxes via the Bowen ratio. However, the IBM method does not account for atmospheric feedbacks to the surface energy balance (Chen and Dirmeyer, 2016). In addition, Rigden & Li (2017) suggested that this method overestimates the contribution of aerodynamic resistance by assuming independence between aerodynamic resistance and the Bowen ratio. To overcome this, Rigden and Li (2017) proposed a new method called the Two-Resistance Mechanism (TRM) method, which replaces the Bowen ratio with the surface resistance. Using the TRM method, Liao et al. (2018) showed that atmospheric feedbacks significantly impact the surface temperature, and therefore need to be accounted for when examining how land use and land cover change affect the surface energy balance. Li and Wang (2019) further demonstrated that atmospheric feedbacks introduce scale-dependence in surface temperature changes induced by land use and land cover change. To date, however, these methods have not been used to study surface energy balance dynamics during springtime, when the surface radiation and energy balance, atmospheric properties, and surface properties are rapidly changing.

In this study, we address two key questions: (1) how does leaf emergence affect surface properties and meteorological conditions across different vegetation types? And (2) what is the relative importance, contribution, and interactions among different land surface and atmospheric variables on springtime changes in surface energy balance? To address these questions, we present an analytical framework based on the TRM method that diagnoses and quantifies the role of key atmospheric and surface biophysical factors in regulating changes in the surface energy balance that occur during the period of leaf emergence. Compared to the original TRM method used in Rigden and Li (2017) and Liao et al. (2018), changes in atmospheric conditions are explicitly and more thoroughly considered in the approach we use here. We apply this revised method to 212 site-years of data from 42 AmeriFlux sites located in the contiguous United States and Eastern Canada that span a wide range of climate regimes and six vegetation types.

2. Methods and data

2.1. Attribution method

We focus on changes in the Bowen ratio (β), which is defined as the ratio of sensible heat flux to latent heat flux. To perform our analysis, we modify the TRM method originally described by Rigden and Li (2017) to account for variations in atmospheric properties such that changes in β can be attributed to changes in surface and atmospheric properties. Specifically, the TRM method starts from the surface radiation and energy balance equations, which are given by

$$R_n = S_{in}(1-\alpha) + \varepsilon L_{in} - \varepsilon\sigma T_s^4 = H + LE + G \tag{1}$$

where R_n is the net surface radiation, S_{in} is the incoming shortwave radiation, α is the surface albedo, ε is the emissivity, L_{in} is the incoming longwave radiation, σ is the Stefan-Boltzmann constant, T_s is the land surface temperature, H is the sensible heat flux, LE is the latent heat flux, and G is the ground heat flux. All symbols used in this study are presented in Appendix A. The sensible and latent heat fluxes are then parameterized using the resistance concepts as follows

$$H = \frac{\rho c_p}{r_a}(T_s - T_a) \tag{2}$$

$$LE = \frac{\rho L_v}{(r_a + r_s)}(q_s^*(T_a) - q_a) \tag{3}$$

where ρ is the air density, c_p is the specific heat of air at constant pressure, r_a is the aerodynamic resistance, T_a is the air temperature, L_v is the latent heat of vaporization, q_s^* is the saturated specific humidity at T_a, q_a is the atmosphere specific humidity, and r_s is the surface or canopy resistance. Substituting H and LE into Eq. (1) and linearizing the outgoing longwave radiation term and the saturated specific humidity term yields analytical expressions for T_s and β

$$T_s = \frac{\lambda_o\left[S_{in}(1-\alpha) + \varepsilon L_{in} - \varepsilon\sigma T_a^4 - G - \frac{\rho L_v}{(r_a+r_s)}(q_a^*(T_a) - q_a)\right]}{1 + \frac{r_o}{r_a}\left[1 + \frac{\delta}{\gamma}\left(\frac{r_a}{r_a+r_s}\right)\right]} + T_a \tag{4}$$

$$\beta = \frac{c_p(T_s - T_a)}{\left(\frac{r_a}{r_a+r_s}\right)L_v(q_s^*(T_a) - q_a)} \tag{5}$$

where $\lambda_o = \frac{1}{4\varepsilon\sigma T_a^3}$, $r_o = \rho c_p \lambda_o$, $\delta = \frac{\partial e^*}{\partial T}|_{T_a}$, $\gamma = \frac{c_p P}{0.622 L_v}$, e^* is the saturation vapor pressure, and P is the air pressure. Substituting T_s into Eq. (5) and taking the first-order derivative of Eq. (5), we obtain the following equation:

$$\Delta\beta = \frac{\partial\beta}{\partial S_{in}}\Delta S_{in} + \frac{\partial\beta}{\partial L_{in}}\Delta L_{in} + \frac{\partial\beta}{\partial q_a}\Delta q_a + \frac{\partial\beta}{\partial T_a}\Delta T_a + \frac{\partial\beta}{\partial G}\Delta G + \frac{\partial\beta}{\partial r_a}\Delta r_a + \frac{\partial\beta}{\partial r_s}\Delta r_s + \frac{\partial\beta}{\partial\alpha}\Delta\alpha \tag{6}$$

In this equation, Δ refers to changes in each variable over time (e.g., $\Delta\alpha = \alpha_{after} - \alpha_{before}$; in this case before and after springtime emergence of leaves) and the partial derivatives (e.g., $\partial\beta/\partial\alpha$) quantify the sensitivity of β to changes in each variable. The analytical expressions for the partial derivatives are too complex to be included here but can be easily obtained numerically (Appendix B provides a link to source codes for this). The novelty of this attribution method is that this approach considers biophysical and atmospheric changes more comprehensively (i.e., inclusion of contributions from changes in specific humidity, albedo, and incoming long- and short-wave radiation) relative to the methods used in Liao et al. (2018) and Rigden and Li (2017).

2.2. Estimation of changes in surface and atmospheric properties

We apply the refined TRM method to 212 site-years of meteorological and flux data from 42 eddy covariance sites located in the conterminous United States and Eastern Canada that span a wide range of climates and six vegetation types: deciduous broadleaf forest, evergreen needleleaf forest, mixed forest, croplands, grasslands, and

Table 1
List of AmeriFlux sites. IGBP denotes the International Geosphere-Biosphere Program land cover type classification: CRO: cropland; DBF: deciduous broadleaf forest; ENF: evergreen needleleaf forest; GRA: grassland; MF: mixed forest; SH: shrubland.

Site Name	Latitude	Longitude	IGBP	Reference
Bondville (US-Bo1)	40.006	−88.290	CRO	Meyers and Hollinger (2004) doi:10.17190/AMF/1,246,036
Bondville Companion site (US-Bo2)	40.009	−88.290	CRO	Bernacchi et al. (2005) doi:10.17190/AMF/1,246,037
Brooks Field Site 10 (US-Br1)	41.975	−93.691	CRO	Chu et al. (2018) doi:10.17190/AMF/1,246,038
Brooks Field Site 11 (US-Br3)	41.975	−93.694	CRO	Chu et al. (2018) doi:10.17190/AMF/1,246,039
Curtice Walter-Berger cropland (US-CRT)	41.629	−83.347	CRO	Chu et al. (2018) doi:10.17190/AMF/1,246,156
Mead Irrigated Continuous Maize (US-Ne1)	41.165	−96.477	CRO	Suyker et al. (2005) doi:10.17190/AMF/1,246,084
Mead Irrigated Maize-Soybean Rotation (US-Ne2)	41.165	−96.470	CRO	Suyker et al. (2005) doi:10.17190/AMF/1,246,085
Mead Rainfed Maize-Soybean Rotation (US-Ne3)	41.18	−96.440	CRO	Suyker et al. (2005) doi:10.17190/AMF/1,246,086
Rosemount G21 (US-Ro1)	44.714	−93.090	CRO	Baker and Griffis (2005) doi:10.17190/AMF/1,246,092
Sioux Falls Portable (US-SFP)	43.241	−96.902	CRO	Euskirchen et al. (2017) doi:10.17190/AMF/1,246,126
Twitchell Alfalfa (US-Tw3)	38.116	−121.647	CRO	Hemes et al. (2019) doi:10.17190/AMF/1,246,149
Twitchell Corn (US-Tw2)	38.105	−121.643	CRO	Baldocchi and Penuelas (2019) doi:10.17190/AMF/1,246,148
Chestnut Ridge (US-ChR)	35.931	−84.332	DBF	Euskirchen et al. (2017) doi:10.17190/AMF/1,246,044
Duke Forest Hardwoods (US-Dk2)	35.974	−79.100	DBF	Oishi et al. (2008) doi:10.17190/AMF/1,246,047
Missouri Ozark Site (US-MOz)	38.744	−92.200	DBF	Wood et al. (2019) doi:10.17190/AMF/1,246,081
Morgan Monroe State Forest (US-MMS)	39.323	−86.413	DBF	Zhang et al. (2018) doi:10.17190/AMF/1,246,080
Oak Openings (US-Oho)	41.555	−83.844	DBF	Chu et al. (2016) doi:10.17190/AMF/1,246,089
Ontario Turkey Point Mature Deciduous (CA-TPD)	42.635	−80.558	DBF	Chu et al. (2018) doi:10.17190/AMF/1,246,152
Silas Little New Jersey (US-Slt)	39.914	−74.596	DBF	Clark et al. (2018) doi:10.17190/AMF/1,246,096
UMBS Disturbance (US-UMd)	45.563	−84.698	DBF	Gough et al. (2013) doi:10.17190/AMF/1,246,134
Michigan Biological Station (US-UMB)	45.56	−84.714	DBF	Gough et al. (2013) doi:10.17190/AMF/1,246,107
Walker Branch Watershed (US-WBW)	35.959	−84.287	DBF	Gu et al. (2008) doi:10.17190/AMF/1,246,109
Duke Forest Loblolly Pine (US-Dk3)	35.978	−79.094	ENF	Oishi et al. (2008) doi:10.17190/AMF/1,246,048
GLEES (US-GLE)	41.367	−106.24	ENF	Frank et al. (2014) doi:10.17190/AMF/1,246,056
GLEES Brooklyn Tower (US-GBT)	41.366	−106.24	ENF	Zeller (2000) doi:10.17190/AMF/1,375,200
Howland Forest (harvest site, US-Ho3)	45.207	−68.725	ENF	Thornton et al. (2002) doi:10.17190/AMF/1,246,063
Howland Forest (main tower, US-Ho1)	45.204	−68.740	ENF	Hollinger et al. (2004) doi:10.17190/AMF/1,246,061
Howland Forest (west tower, US-Ho2)	45.209	−68.747	ENF	Xiao et al. (2004) doi:10.17190/AMF/1,246,062
Mary's River (Fir) site (US-MRf)	44.647	−123.552	ENF	Kwon et al. (2018) doi:10.17190/AMF/1,246,049
NC Clearcut#3 (US-NC3)	35.799	−76.656	ENF	Euskirchen et al. (2017) doi:10.17190/AMF/1,419,506
NC Loblolly Plantation (US-NC2)	35.803	−76.669	ENF	Noormets et al. (2010) doi:10.17190/AMF/1,246,083
Ontario Turkey Point 1939 Plantation (CA-TP4)	42.710	−80.357	ENF	Peichl et al. (2010) doi:10.17190/AMF/1,246,012
Brookings (US-Bkg)	44.345	−96.836	GRA	Gilmanov et al. (2005) doi:10.17190/AMF/1,246,040
Canaan Valley (US-CaV)	39.063	−79.421	GRA	Euskirchen et al. (2017) doi:10.17190/AMF/1,246,042
Cottonwood (US-Ctn)	43.95	−101.847	GRA	Euskirchen et al. (2017) doi:10.17190/AMF/1,246,117
Duke Forest Open Field (US-Dk1)	35.971	−79.093	GRA	Oren et al. (2006) doi:10.17190/AMF/1,246,046
Goodwin Creek (US-Goo)	34.255	−89.874	GRA	Runkle et al. (2017) doi:10.17190/AMF/1,246,058
Kansas Field Station (US-KFS)	39.056	−95.191	GRA	Wolf et al. (2016) doi:10.17190/AMF/1,246,132
KUOM Turfgrass Field (US-KUT)	44.995	−93.186	GRA	Hiller et al. (2011) doi:10.17190/AMF/1,246,145
Ontario Groundhog River (CA-Gro)	48.217	−82.156	MF	McCaughey et al. (2006) doi:10.17190/AMF/1,245,996
RCEW Mountain Big Sagebrush (US-Rms)	43.065	−116.749	SH	Euskirchen et al. (2017) doi:10.17190/AMF/1,375,202
NC Clearcut (US-NC1)	35.812	−76.712	SH	Noormets et al. (2012) doi:10.17190/AMF/1,246,082

shrublands (Table 1). Liao et al. (2018) found that the TRM-based attribution cannot be applied to data at half-hourly time scale because the available energy (i.e., the sum of sensible and latent heat fluxes) outside of the mid-day periods can be quite low, thus some modeled quantities during these periods, especially the aerodynamic and surface resistance terms, can have high uncertainties in the 30-min data. By computing daily averages, these uncertainties are reduced. Hence, in this study, we aggregate the 30-min data to daily averages using data from daytime conditions when incoming shortwave radiation is larger than 25 W m^{-2}. We also remove any data for which the estimated resistances are negative at daily scale. To measure changes before and after leaf emergence, we use the daily data to estimate mean daily values for 30-day periods before and after leaf emergence at each site, and perform our attribution analysis based on these data.

All the inputs needed for the attribution analysis are estimated using data from the AmeriFlux database (https://ameriflux.lbl.gov; Table 1) following Wang et al. (2019). In particular, aerodynamic and surface resistances are inferred from sensible and latent heat flux measurements, as well as temperature and humidity measurements, using Eqs. (2) and (3). Ground heat fluxes are assigned the residual of the surface energy balance to ensure surface energy budget closure. Hence the contribution of ground heat flux implicitly includes the role of surface energy imbalance or non-closure (see Foken 2008 for review). Where available, we use the soil heat flux measurements to represent ground heat flux, which are available at 34 out of 42 sites. As we show below, the results are not significantly affected in either case due to the small sensitivity of Bowen ratio to changes in ground heat flux.

2.3. Optimization of attribution method

Prior to applying the attribution method, we optimize our procedure for estimating partial derivatives using a weighted average approach described by Liao et al. (2018). This is needed because the attribution method is based on first-order Taylor series expansions that neglect higher-order and cross-order terms. Hence, this approach is acceptable only if changes in the attribution variables are small. However, because changes in land surface and atmospheric properties can be significant during springtime, the partial derivatives estimated

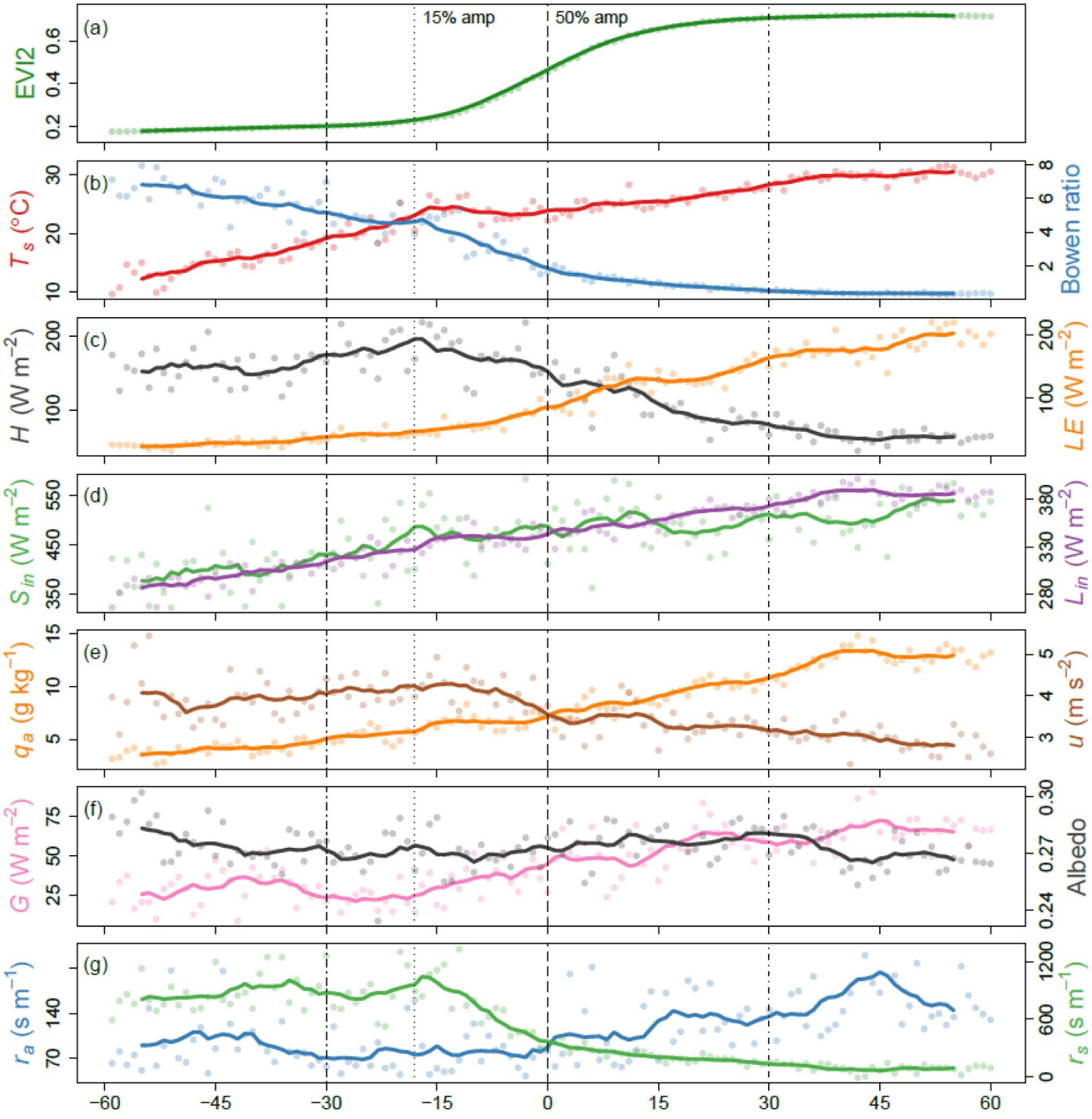

Fig. 1. Changes in biophysical and meteorological properties 60 days before and after leaf emergence at the Morgan-Monroe State Forest site averaged from 2001 to 2014. EVI2, T_s, H, LE, S_{in}, L_{in}, q_a, u, G, r_a, and r_s represent vegetation index, land surface temperature, sensible heat flux, latent heat flux, incoming shortwave radiation, incoming longwave radiation, specific humidity, wind speed, ground heat flux, aerodynamic resistance, and surface resistance, respectively. Dots and lines represent 14-year averaged values and 10-day moving averages, respectively. Vertical dotted lines near 15 days before leaf emergence represent 15% of the seasonal EVI2 amplitude. Note that the values are estimated from daytime conditions.

at the reference state (in this case before the emergence of leaves) can cause large errors in modeled changes in the Bowen ratio (Liao et al., 2018). To account for this, we optimize the partial derivatives for each site so that the calculated root-mean-square errors for changes in β are minimized. Specifically, the partial derivatives in the attribution model are calculated as

$$X = \frac{X_{before} + mX_{after}}{1 + m} \tag{7}$$

where X is the final partial derivative used in the model, m is the average weight, and X_{before} and X_{after} are the partial derivatives calculated only using data from time periods before and after springtime phenology, respectively.

2.4. Springtime phenology

The timing of springtime leaf emergence is identified at each site using the Collection 6 MODIS Land Cover Dynamics (i.e., land surface phenology) product (MCD12Q2; Moon et al., 2019). A number of studies have evaluated the MODIS phenology algorithm and have demonstrated that it shows good agreement with ground-based phenophase transition observations (Ganguly et al., 2010; Richardson et al., 2018). The algorithm uses panelized cubic splines to interpolate daily time series of the two-band Enhanced Vegetation Index (EVI2) at each 500 m pixel, which is computed from the Collection 6 MODIS normalized BRDF-adjusted surface reflectance (NBAR) values (MDC43A4; Wang et al., 2018). In the MCD12Q2 product, phenological transition dates are estimated to occur when the EVI2 time series at each pixel cross assigned thresholds in the seasonal amplitude of EVI2. In this study, we define the timing of leaf emergence as the day of year when EVI2 time series cross 50% of the seasonal amplitude during the "green-up" phase. Note that even though the timing of 15% of the seasonal amplitude provides a closer approximation of the timing of leaf emergence (as shown Fig. 1a), we use 50% as the threshold because sensible and latent heat fluxes around the 15% threshold tend to be small, which can introduce large uncertainties in the inferred variables, especially aerodynamic and surface resistances. Lastly, to minimize errors from geolocation and product uncertainty, we use the average green-up date from 3 by 3 windows of MODIS pixels centered over each flux tower location.

2.5. Attribution of changes in aerodynamic resistance

In Section 3.3, we attribute changes in aerodynamic resistance (r_a) following the basic approach used to attribute changes in β (Eq. (6)). Using Monin-Obukhov similarity theory, r_a can be parameterized as a function of wind speed (u), momentum roughness length (z_o), and thermal roughness length (z_{oh}):

$$r_a = \frac{1}{\kappa^2 u}\left[\ln\left(\frac{z-d}{z_o}\right) - \Psi_m\left(\frac{z-d}{L}\right) + \Psi_m\left(\frac{z_o}{L}\right) + \hat{\Psi}_m(z, L)\right] \left[\ln\left(\frac{z-d}{z_{oh}}\right) - \Psi_h\left(\frac{z-d}{L}\right) + \Psi_h\left(\frac{z_{oh}}{L}\right) + \hat{\Psi}_h(z, L)\right] \quad (8)$$

where κ is the von-Karman constant, z is the measurement height, d is the displacement height (assumed to be 70% of the vegetation height), L is the Obukhov length, and Ψ_m and Ψ_h are stability correction functions for momentum and heat, respectively, based on the Businger-Dyer relations (Brutsaert, 2005; Garratt, 1992). The correction functions $\hat{\Psi}_m(z, L)$ and $\hat{\Psi}_h(z, L)$ are included to account for roughness sublayer effects for momentum and heat, respectively (Arnqvist and Bergström, 2015; Harman and Finnigan, 2007). To use Eq. (8), we need to estimate the changes in roughness lengths, atmospheric stabilities, and roughness sublayers. The roughness lengths are estimated following Rigden et al. (2018), but including the correction for roughness sublayer. For atmospheric stabilities, the Obukhov length is defined as

$$L = \frac{-u_*^3 \rho T_a (1 + \eta q_a) c_p}{\kappa g H} \quad (9)$$

where u_* is the friction velocity, η (= 0.61) is the dimensionless ratio of the gas constants for dry air to water vapor, and g is the gravitational acceleration. The stability correction functions Ψ_m and Ψ_h are then calculated from the dimensionless stability parameter ξ (= z/L) as follows, with $x = (1 - 16\xi)^{1/4}$:

$$\Psi_m = \begin{cases} \ln\left[\left(\frac{1+x^2}{2}\right)\left(\frac{1+x}{2}\right)^2\right] - 2\tan^{-1}x + \frac{\pi}{2} \text{ for } \xi < 0 \\ -5\xi \text{ for } \xi \geq 0 \end{cases} \quad (10)$$

$$\Psi_h = \begin{cases} 2\ln\left(\frac{1+x^2}{2}\right) \text{ for } \xi < 0 \\ -5\xi \text{ for } \xi \geq 0 \end{cases} \quad (11)$$

The roughness sublayer correction functions $\hat{\Psi}_m(z, L)$ and $\hat{\Psi}_h(z, L)$ are calculated following De Ridder (2010) as

$$\hat{\Psi}_i(z, L) = \Phi_i\left[\left(1 + \frac{\nu}{\mu_i z/z_*}\right)\frac{z}{L}\right]\frac{1}{\lambda}\ln\left(1 + \frac{\lambda}{\mu_i z/z_*}\right)e^{-\mu_i z/z_*} \quad (12)$$

where i is an index indicating momentum (m) or heat (h) and Φ is the surface-layer stability function defined in De Ridder (2010). ν, μ, and λ are the correction coefficients and z_* is the roughness sublayer height above the displacement height, and we use these parameters as constants with values from De Ridder (2010). Taking the derivative of Eq. (8), we obtain the following equation:

$$\Delta r_a = \frac{\partial r_a}{\partial u}\Delta u + \left(\frac{\partial r_a}{\partial \Psi_m}\Delta\Psi_m + \frac{\partial r_a}{\partial \Psi_h}\Delta\Psi_h + \frac{\partial r_a}{\partial L}\Delta L + \frac{\partial r_a}{\partial \hat{\Psi}_m}\Delta\hat{\Psi}_m + \frac{\partial r_a}{\partial \hat{\Psi}_h}\Delta\hat{\Psi}_h\right) + \left(\frac{\partial r_a}{\partial z_o}\Delta z_o + \frac{\partial r_a}{\partial z_{oh}}\Delta z_{oh}\right) \quad (13)$$

Hence, Eq. (13) quantifies the relative contributions from changes in wind speed (the first term, right-hand side of Eq. (13)), atmospheric stability including roughness sublayer corrections (second term), and roughness lengths for heat and momentum (third term) to changes in aerodynamic resistance. We apply this method to data from 10 deciduous broadleaf forest sites, where vegetation height information is available and where vegetation heights are relatively stable compared to other vegetation types (e.g., croplands) during springtime.

3. Results and discussion

3.1. Changes in surface and atmospheric properties during springtime

To illustrate springtime dynamics typical of those observed at AmeriFlux sites included in our analysis, Fig. 1 shows daily values of biophysical and meteorological properties during a 120-day period centered on the timing of leaf emergence at the Morgan-Monroe State Forest site (US-MMS, DBF), averaged from 2001 to 2014. Vegetation index (i.e., EVI2) values estimated from MODIS are also shown, which increase gradually throughout the springtime. Land surface temperature (T_s) increases throughout the springtime, although the rate of change decreases around the time when EVI2 values start to increase (i.e., around −15 days on the x-axis of Fig. 1). Similarly, the daytime Bowen ratio (β) decreases monotonically throughout the spring period, with a distinct drop around the time that the rate of change in T_s decreases. Radiation forcing (i.e., incoming shortwave and longwave radiation) and specific humidity also increase monotonically during springtime, and ground heat flux and albedo are relatively constant. Surface resistance and wind speed decrease sharply after leaf emergence, while aerodynamic resistance increases after leaf emergence (i.e., around 0 on the x-axis of Fig. 1). Note that the surface resistance drops consistently (over more than a month) during the springtime in proportion to EVI2 increase, which is consistent with the pattern previously reported by Sakai et al. (1997).

In general, the patterns shown in Fig. 1 are consistent across all of the plant functional types included in our analysis (Table 2). On

Table 2
Springtime phenology and changes in biophysical and meteorological properties after leaf emergence. Values in parentheses indicate one standard deviation.

Vegetation Type	Number of site-years	Springtime phenology (day of year)	ΔIncoming shortwave radiation (W m^{-2})	ΔIncoming longwave radiation (W m^{-2})	ΔSpecific humidity (g kg^{-1})	ΔAir temperature (°C)	ΔGround heat flux (W m^{-2})	ΔAerodynamic resistance (s m^{-1})	ΔSurface resistance (s m^{-1})	ΔAlbedo (-)	ΔWind speed (m s^{-1})
Deciduous broadleaf forest	66	125 (12)	25 (62)	31 (15)	3.1 (1.5)	4.9 (3.1)	14 (19)	15 (18)	−315 (95)	−0.001 (0.020)	−0.6 (0.4)
Evergreen needleleaf forest	43	142 (21)	15 (76)	31 (17)	2.8 (1.4)	4.8 (2.4)	−9 (8)	3 (8)	−43 (82)	−0.015 (0.021)	−0.4 (0.5)
Mixed forest	10	154 (6)	0 (42)	38 (11)	3.3 (1.0)	5.9 (2.2)	10 (9)	23 (9)	−138 (83)	−0.001 (0.009)	−0.5 (0.5)
Cropland	68	160 (21)	34 (50)	23 (14)	3.2 (1.7)	3.6 (2.4)	13 (39)	36 (39)	−232 (214)	−0.019 (0.033)	−1.2 (0.9)
Grassland	20	124 (16)	−15 (80)	32 (19)	3.2 (1.7)	4.1 (3.0)	10 (49)	43 (49)	−132 (70)	−0.034 (0.024)	−0.6 (0.6)
Shrubland	5	123 (7)	−35 (65)	35 (15)	3.1 (1.0)	3.0 (2.0)	13 (8)	17 (8)	−142 (102)	−0.022 (0.017)	−0.4 (0.4)

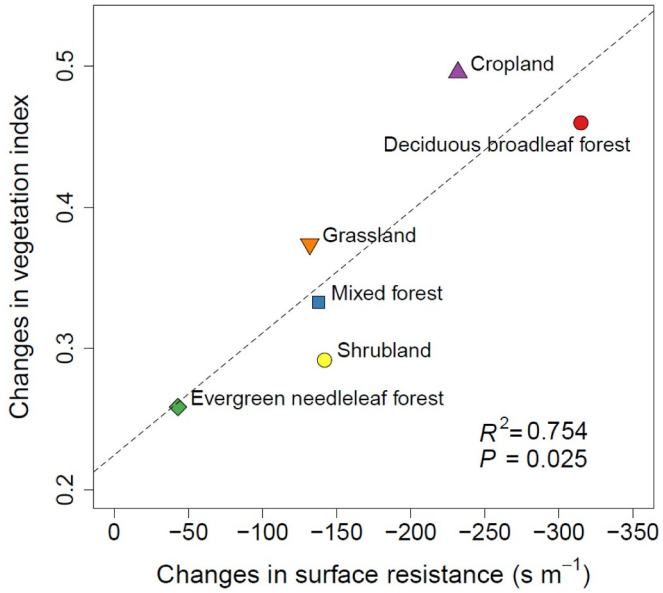

Fig. 2. Relationship between changes in surface resistance and vegetation index (EVI2). Each point represents the average change for each vegetation type. Changes in EVI2 values are computed based on the average EVI2 value in 3 by 3 MODIS pixel windows centered over each flux tower.

average, incoming longwave radiation, air temperature, specific humidity, and aerodynamic resistance all increase during springtime, while surface resistance decreases. Changes in ground heat flux and albedo are fairly small. In addition, wind speed generally decreases during springtime across all vegetation types, including evergreen needleleaf forest sites where changes in surface properties are modest.

However, there are notable differences in specific terms across vegetation types. In particular, deciduous broadleaf forests and croplands exhibited the largest decreases in surface resistance, followed by shrublands, mixed forests, grasslands, and evergreen needleleaf forests (Table 2). Unsurprisingly, some of these differences are caused by differences in the magnitude of seasonal variation in leaf area across vegetation types. Fig. 2 shows that observed decreases in surface resistance across vegetation types are strongly correlated with the amplitude of seasonal variation in EVI2 values over the growing season ($R^2 = 0.754$, $p = 0.025$).

3.2. Attribution of decreases in the Bowen ratio

The TRM framework provides an effective framework for decomposing and quantifying the relative contributions of land surface and atmospheric properties to changes in the surface energy balance (e.g., Li et al., 2019; Liao et al., 2018). In this study, we refine the TRM method to incorporate associated changes in surface properties as well as atmospheric conditions more thoroughly (i.e., inclusion of the effects of changes in specific humidity, albedo, and two incoming radiations). Fig. 3 shows results from this method that attribute changes in β to contributions from changes in surface properties and atmospheric conditions. Each panel presents results summarized by vegetation type.

As leaves emerge, partitioning of available energy increasingly favors latent heat flux from transpiration. This is reflected in the strong negative contributions from changes in surface resistance to the Bowen ratio as shown in Fig. 3. In our study, the surface resistance is parameterized using a simple big-leaf representation and hence includes both soil and vegetation conditions, which has been traditionally parameterized as a function of leaf area and various stressors (e.g., soil water content and vapor pressure deficit; Jarvis et al., 1976; Monteith and Unsworth, 2013; Stewart, 1988). Fig. 2 shows that the observed springtime decrease in surface resistance is largely caused by

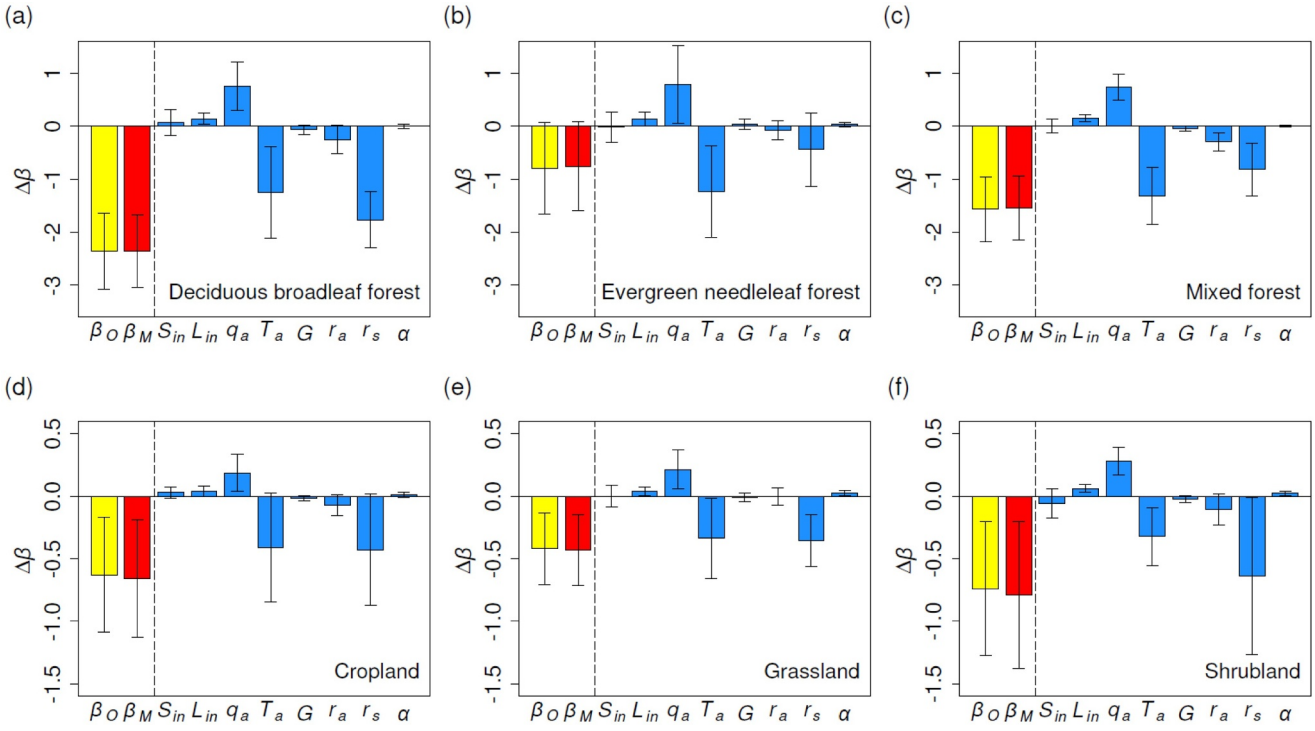

Fig. 3. Attribution of the Bowen ratio change after springtime phenology. β_O and β_M are the observed and modeled changes in Bowen ratio, respectively. S_{in}, L_{in}, q_a, T_a, G, r_a, r_s, and α represent contributions from changes in incoming shortwave radiation, incoming longwave radiation, specific humidity, air temperature, ground heat flux, aerodynamic resistance, surface resistance, and albedo, respectively. Different panels present results for different vegetation types. The error bars show one standard deviation from the mean. Note the difference in the scale of the y-axis between panels a-c and panels d-f.

Table 3
The 30-days averaged daytime Bowen ratio before and after springtime phenology and their differences for different vegetation types. Values in parentheses indicate one standard deviation.

Vegetation type	Before	After	Difference
Deciduous broadleaf forest	3.20 (0.79)	0.85 (0.27)	−2.35 (0.72)
Evergreen needleleaf forest	2.01 (1.12)	1.22 (0.49)	−0.79 (0.87)
Mixed forest	2.39 (0.71)	0.83 (0.20)	−1.56 (0.61)
Cropland	1.13 (0.62)	0.50 (0.37)	−0.63 (0.46)
Grassland	0.86 (0.44)	0.44 (0.24)	−0.42 (0.29)
Shrubland	1.39 (0.72)	0.65 (0.20)	−0.74 (0.53)

increases in leaf area, suggesting that the surface resistance in our analysis primarily reflects the surface biophysical conditions instead of atmospheric conditions.

Our results also demonstrate that decreases in β are the product of interplay among a number of related variables rather than being regulated by a single element such as changes in leaf area. For example, atmospheric evaporative demand increases as air temperature increases, which increases evapotranspiration and decreases β. Concurrently, increases in specific humidity impose a negative feedback on evaporative fluxes, which partly offsets the influence of higher air temperatures and lower surface resistances. The contributions of aerodynamic resistance are consistently negative (i.e., they act to decrease β), implying that larger aerodynamic resistance tends to inhibit sensible heat flux more strongly than latent heat flux. While these features are quite consistent across vegetation types, the magnitude of $\Delta\beta$ is quite different, with deciduous broadleaf forests showing the largest changes in β versus other vegetation types (i.e., larger decreases in DBF and MF

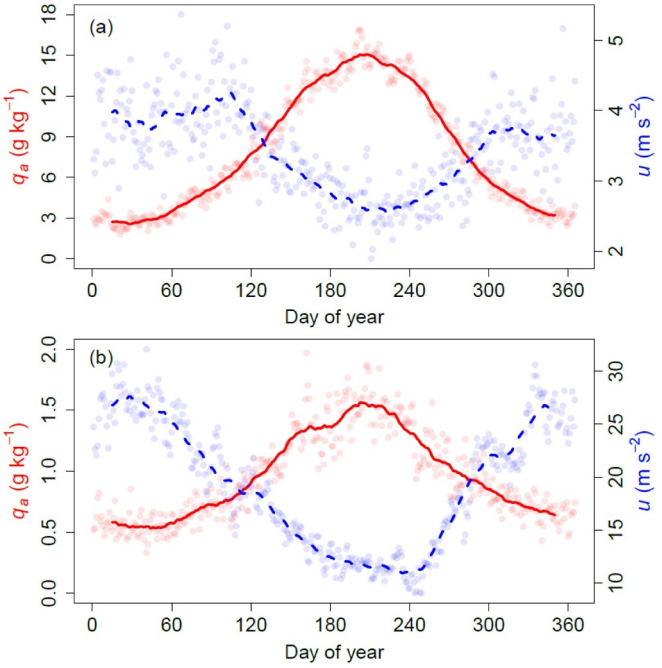

Fig. 4. Annual patterns in specific humidity (q_a; red dots and solid lines) and wind speed (u; blue dots and dashed lines) at the Morgan-Monroe State Forest site measured from a flux tower (a) and at 500 hPa across the northeastern United States from the MERRA reanalysis data (b). Dots and lines represent 10-year averaged values (i.e., from 2001 to 2010) and 30-day moving averages, respectively. Note the values are estimated from daytime conditions.

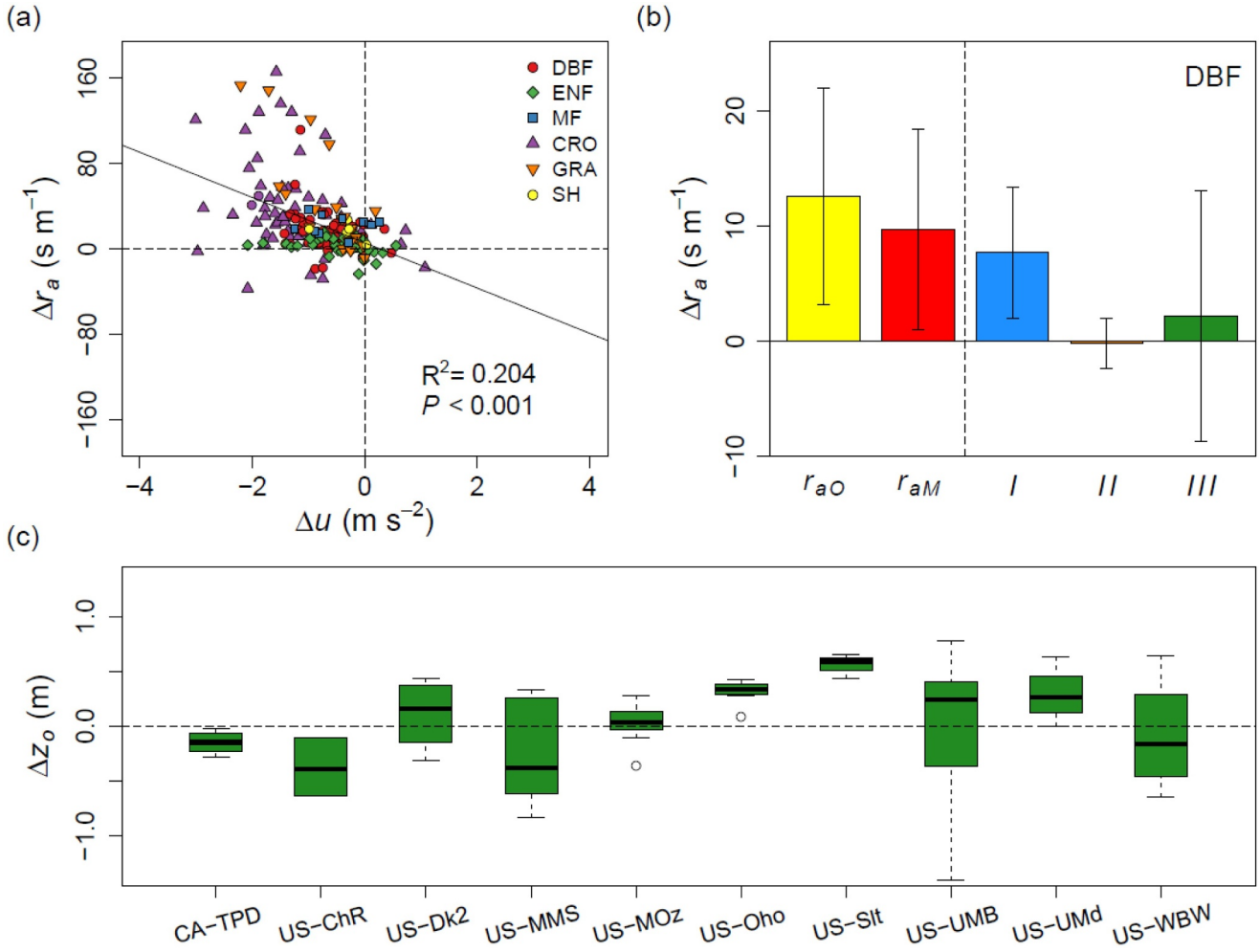

Fig. 5. The relationship between changes in wind speed (Δu) and changes in aerodynamic resistance (Δr_a) (a), attribution of changes in aerodynamic resistance (b), and changes in momentum roughness length (Δz_o) (c) at 10 deciduous broadleaf forest sites. Note that the aerodynamic resistance was estimated from sensible heat flux, land surface temperature, and air temperature; hence Δu and Δr_a are quantified independently from each other. In panel (b), r_{aO} and r_{aM} represent the observed and modeled aerodynamic resistance changes, respectively, and *I, II*, and *III* represent contributions from changes in wind speed, atmospheric stability including roughness sublayer corrections, and roughness length (see Eq. (13)); the error bars show one standard deviation from the mean.

than in ENF, CRO, CRA, and SH, Fig. 3). This result is partly related to the fact that different vegetation types have different magnitudes of increase in leaf area (see Fig. 2) and also that β tends to be larger prior to leaf emergence at forested sites (especially at DBF sites) than at non-forest sites (Table 3).

In contrast, the influence of changes in shortwave and longwave radiation, ground heat flux, and albedo on β are small. For radiative fluxes, because β is the ratio of the two turbulent flux terms (i.e. the Bowen ratio), the impact of changes in radiation on β is expected to be small. In addition, the small influence from ground heat flux suggests that lack of surface energy balance closure is not important in our attribution analysis. Recall that we calculated the ground heat flux at each site as residual of the surface energy. In parallel, we also conducted the same analysis using soil heat flux measurements for the 34 sites where soil heat flux measurements were available, which yielded almost identical results (c.f. Fig. C.1 and Fig. 3). Hence, we conclude that the energy closure (or lack thereof) is not a significant factor in our analysis.

The results presented in this section are consistent with existing theory and results from previous empirical studies (e.g., Moore et al., 1996; Schwartz and Crawford, 2001; Wilson and Baldocchi, 2000), but reveal several interesting features regarding the impact of changing atmospheric conditions on the surface energy balance. For example, changes in specific humidity impose a positive contribution to the Bowen ratio, implying that increases in specific humidity reduce the evaporative fluxes. This is unsurprising because increasing specific humidity arising from increasing evapotranspiration causes the gradient of specific humidity between the land surface and the boundary layer to decrease, thereby imposing a negative feedback on evapotranspiration (Brutsaert, 1982; Heerwaarden et al., 2009; Jarvis and McNaughton, 1986; Monteith and Unsworth, 2013; Santanello et al., 2018). However, the degree to which changes in specific humidity are solely attributable to local processes versus larger-scale weather patterns is unclear.

To address whether changes in near-surface atmospheric properties reflect local boundary layer feedbacks or changes in large-scale forcing,

we compared 10-year averaged annual patterns (from 2001 to 2010) in specific humidity and wind speed at the Morgan-Monroe State Forest flux site against corresponding values at 500 hPa (~5500 m above sea level) across the northeastern United States (i.e., Latitude: 35°~45°; Longitude: −99°~−78°) from the Modern-Era Retrospective analysis for Research and Applications (MERRA) Version 2 data set (Rienecker et al., 2011). As shown in Fig. 4, seasonal variation in these variables are quite similar (i.e., low in wintertime and high in summertime for specific humidity, and vice versa for wind speed). Note that we also examined wind patterns based on MERRA data at 850 hPa (not shown) and found similar results. At 500 hPa, atmospheric properties are expected to be unaffected by local-scale surface properties. Hence we assert that the changes in specific humidity and wind speed that we observe in AmeriFlux data are not entirely controlled by local boundary layer feedbacks. Although this type of empirical analysis does not provide a direct attribution of local versus large-scale influences on near-surface atmospheric properties, it strongly implies that changes in atmospheric properties are not exclusively determined locally by changes in surface properties (Fitzjarrald et al., 2001; McNaughton and Spriggs, 1986).

Characterization and quantification of the functional relationship between near-surface atmospheric properties and large-scale forcing by atmospheric processes (i.e., above the boundary layer) are complex and beyond the scope of this study. Doing so empirically would require (at a minimum) vertical profile measurements of potential temperature, specific humidity, and wind speed (van Heerwaarden et al., 2010; Wouters et al., 2019; Zhang et al., 2019), which were not available at the flux tower sites included in this study. Model-based approaches using (for e.g.,) convective boundary layer models have previously been used to link near-surface atmospheric properties with land surface conditions and large-scale atmospheric forcing (e.g., Gentine et al., 2016; Jacobs and De Bruin, 1992; Juang et al., 2007; McNaughton and Spriggs, 1986; van Heerwaarden et al., 2010). The application of these models, combined with observations collected at flux tower sites, have potential to shed further insight into this question but is left for future research.

3.3. Attribution of increases in aerodynamic resistance: the role of wind speed

An additional important empirical result from our analysis is that aerodynamic resistance increases during springtime across all six vegetation types (Table 2). Previous studies have interpreted this change to reflect increases the surface roughness length, which lowers aerodynamic resistance (e.g., Bonan, 2015; Peñuelas et al., 2009). To illustrate why this is not the case, Fig. 5a plots changes in aerodynamic resistance against changes in wind speed across all site-years included in our analysis, and clearly shows that wind speed decreases for almost every site-year and that increases in aerodynamic resistance are negatively correlated with decreases in wind speed. One interpretation of this result is that the emergence of leaves and associated changes in surface three-dimensional structure act to effectively increase surface roughness (via, e.g., increasing the momentum roughness length), leading to lower near-surface wind speeds.

However, this does not appear to be the case. Fig. 5b shows results from applying the attribution method described in Section 2.5 to data from the 10 deciduous broadleaf forest sites included in our analysis. As this figure shows, changes in aerodynamic resistance are mainly attributable to changes in wind speed, with only small contributions from changes in atmospheric stability and roughness length. Further, we find no consistent pattern of springtime changes in the momentum roughness length across these ten deciduous broadleaf forests sites (Fig. 5c), which contradicts traditional models that the momentum roughness length increases after leaf emergence (Peñuelas et al., 2009; Richardson et al., 2013). Conversely, our results are consistent with previous studies demonstrating that the momentum roughness length does not increase monotonically with leaf area index (Blanken and Black, 2004; Garratt, 1992; Parker and Russ, 2004; Sakai et al., 1997; Shaw and Pereira, 1982). When vegetation density is low, increasing leaf area does generally increase the momentum roughness length. In forests, however, where the vegetation density is already high, increasing leaf area index may cause the momentum roughness length to decrease because the vegetation canopy becomes more compact and the surface effectively becomes smoother. In other words, mature canopies can be aerodynamically smoother than their leafless state, depending on the canopy surface rugosity (Blanken and Black, 2004; Parker and Russ, 2004). As a consequence, we conclude that observed increases in aerodynamic resistance after leaf emergence are mainly induced by seasonal decreases in synoptic-scale wind speed (Fig. 4) rather than by changes in land surface roughness lengths.

4. Conclusions

In this paper, we present a physically-based attribution method, which provides a powerful approach for separating and quantifying the differential impacts of concurrent and interacting changes in surface and atmospheric properties on the surface energy balance, and apply it to data from a large number of sites covering a wide range of climates and vegetation types. The results presented here suggest that changes in surface biophysical properties and energy balance during springtime phenology are strongly coupled with atmospheric processes. Specifically, the springtime decrease in the Bowen ratio, which quantifies energy partitioning into sensible and latent heat fluxes, is the result of interactions among changes in surface conditions and atmospheric properties. While changes in surface resistance and air temperature effectively decrease the Bowen ratio, increases in near-surface specific humidity impose a negative feedback on evaporative fluxes. Further, observed increases in aerodynamic resistance are mainly attributable to reductions in wind speed that are not solely related to changes in surface properties. Our study highlights that observed changes in near-surface meteorological properties such as specific humidity and wind speed are not entirely controlled by local processes but seem to strongly follow changes in large-scale atmospheric properties. More broadly, the physically-based method used in this study provides a useful way to unravel the relative importance of different variables on surface energy balance dynamics.

Declaration of Competing Interest

None.

Acknowledgments

This research was funded by NSF grant #EF-1702627 (“Improved Understanding of Feedbacks between Ecosystem Phenology and the Weather-Environment Nexus at Local-to-Continental Scales”). We thank the AmeriFlux primary investigators of the sites used in this study. AmeriFlux data are available at http://ameriflux.lbl.gov.

Appendix A

Table A.1.

Table A.1
List of symbols.

Abbreviation	Definition	Units
β	Bowen ratio	–
R_n	Net surface radiation	W m^{-2}
S_{in}	Incoming shortwave radiation	W m^{-2}
L_{in}	Incoming longwave radiation	W m^{-2}
H	Sensible heat flux	W m^{-2}
LE	Latent heat flux	W m^{-2}
G	Ground heat flux	W m^{-2}
T_a	Air temperature	K
T_s	Land surface temperature	K
q_a	Specific humidity	g kg^{-1}
r_a	Aerodynamic resistance	s m^{-1}
r_s	Surface resistance	s m^{-1}
P	Air pressure	Pa
u	Wind speed	m s^{-1}
u_*	Friction velocity	m s^{-1}
α	Surface albedo	–
ε	emissivity	–
ρ	Air density	kg m^{-3}
σ	Stefan-Boltzmann constant	W m^{-2} K^{-4}
κ	von-Karman constant	–
c_p	Specific heat of air	J kg^{-1} K^{-1}
L_v	Latent heat of vaporization	J kg^{-1}
q_s^*	Saturated specific humidity	g kg^{-1}
g	Gravitational acceleration	m s^{-2}
e^*	Saturation vapor pressure	Pa
z	Measurement height	M
z_o	Momentum roughness length	M
z_{oh}	Thermal roughness length	M
z_*	Roughness sublayer height above the displacement height	M
d	Displacement height	M
L	Obukhov length	M
Ψ_m	Stability correction function for momentum	–
Ψ_h	Stability correction function for heat	–
$\hat{\Psi}_m$	Roughness sublayer correction function for momentum	–
$\hat{\Psi}_h$	Roughness sublayer correction function for heat	–
Φ	surface-layer stability function	–
η	Ratio of the gas constants for dry air to water vapor	–
ν	Coefficient in the approximated roughness sublayer correction	–
μ	Coefficient in the approximated roughness sublayer correction	–
λ	Coefficient in the approximated roughness sublayer correction	–

Appendix B. Source codes

The source codes used in this study are available in a GitHub repository:
https://github.com/minkyum/lseb

Appendix C

Fig. C.1.

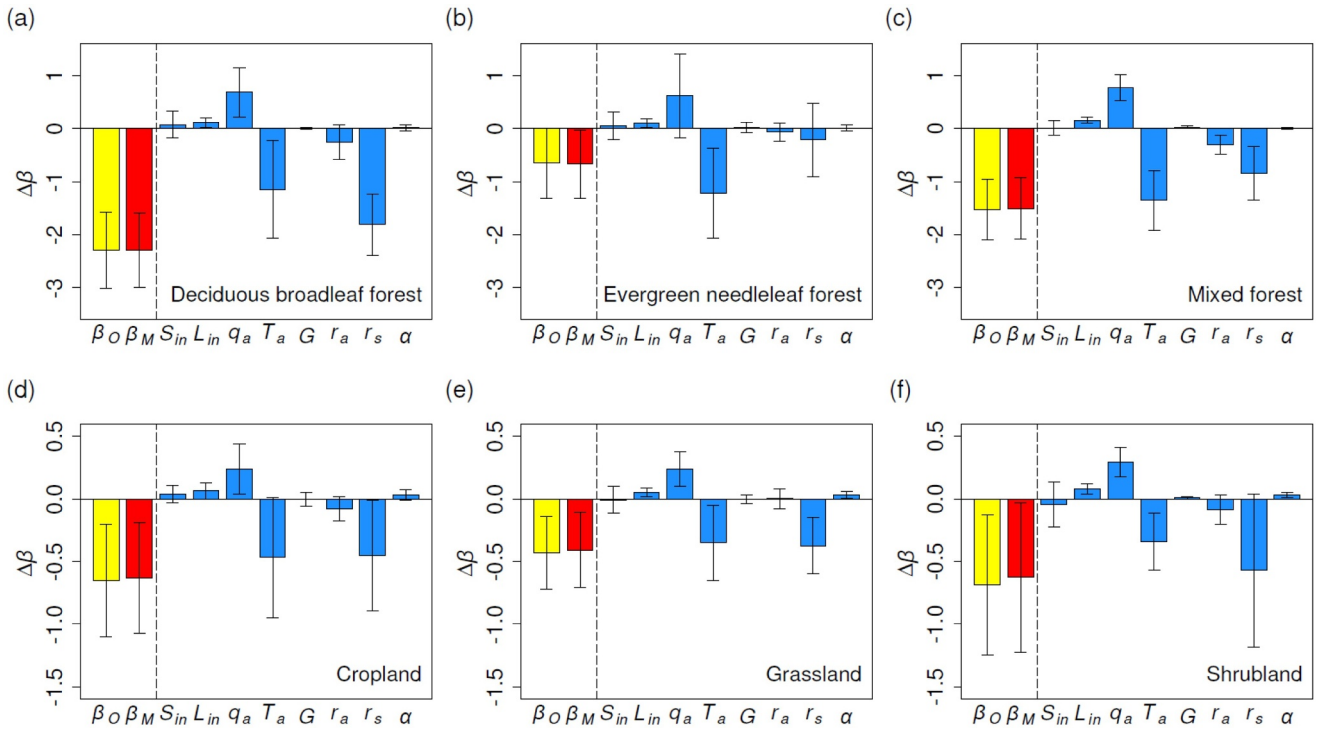

Fig. C.1. Same as Fig. 3. but the analysis is conducted using measured soil heat fluxes for *G*, which are only available at 34 out of 42 sites.

References

Arnqvist, J., Bergström, H., 2015. Flux-profile relation with roughness sublayer correction. Q. J. R. Meteorol. Soc. 141, 1191–1197. https://doi.org/10.1002/qj.2426.

Baker, J.M., Griffis, T.J., 2005. Examining strategies to improve the carbon balance of corn/soybean agriculture using eddy covariance and mass balance techniques. Agric. Forest Meteorol. 128, 163–177. https://doi.org/10.1016/j.agrformet.2004.11.005.

Bernacchi, C.J., Hollinger, S.E., Meyers, T., 2005. The conversion of the corn/soybean ecosystem to no-till agriculture may result in a carbon sink. Glob, Chang Biol, 11, 1867–1872. https://doi.org/10.1111/j.1365-2486.2005.01050.x.

Blanken, P.D., Black, T.A., 2004. The canopy conductance of a boreal aspen forest, Prince Albert National Park, Canada. Hydrol. Process. 18, 1561–1578. https://doi.org/10.1002/hyp.1406.

Bonan, G., 2015. Ecological Climatology: Concepts and Applications, 3rd ed. Cambridge University Press.

Bonan, G.B., 2008. Forests and climate change: forcings, feedbacks, and the climate benefits of forests. Science 320, 1444–1449. https://doi.org/10.1126/science.1155121.

Brutsaert, W., 2005. Hydrology: an Introduction. Cambridge University Press, CambridgeNew York.

Brutsaert, W., 1982. Evaporation Into the Atmosphere: Theory, History and Applications. Springer Science & Business Media.

Chen, L., Dirmeyer, P.A., 2016. Adapting observationally based metrics of biogeophysical feedbacks from land cover/land use change to climate modeling. Environ. Res. Lett. 11, 034002. https://doi.org/10.1088/1748-9326/11/3/034002.

Chu, H., Baldocchi, D.D., Poindexter, C., Abraha, M., Desai, A.R., Bohrer, G., Arain, M.A., Griffis, T., Blanken, P.D., O'Halloran, T.L., Thomas, R.Q., Zhang, Q., Burns, S.P., Frank, J.M., Christian, D., Brown, S., Black, T.A., Gough, C.M., Law, B.E., Lee, X., Chen, J., Reed, D.E., Massman, W.J., Clark, K., Hatfield, J., Prueger, J., Bracho, R., Baker, J.M., Martin, T.A., 2018. Temporal dynamics of aerodynamic canopy height derived from eddy covariance momentum flux data across North American flux networks. Geophys. Res. Lett. 45, 9275–9287. https://doi.org/10.1029/2018GL079306.

Chu, H., Chen, J., Gottgens, J.F., Desai, A.R., Ouyang, Z., Qian, S.S., 2016. Response and biophysical regulation of carbon dioxide fluxes to climate variability and anomaly in contrasting ecosystems in northwestern Ohio, USA. Agric. Forest Meteorol. 220, 50–68. https://doi.org/10.1016/j.agrformet.2016.01.008.

Chuine, I., de Cortazar-Atauri, I.G., Kramer, K., Hänninen, H., 2013. Plant development models. In: Schwartz, M.D. (Ed.), Phenology: An Integrative Environmental Science. Springer, Netherlands, Dordrecht, pp. 275–293. https://doi.org/10.1007/978-94-007-6925-0_15.

Clark, K.L., Renninger, H.J., Skowronski, N., Gallagher, M., Schäfer, K.V.R., 2018. Decadal-Scale reduction in forest net ecosystem production following insect defoliation contrasts with short-term impacts of prescribed fires. Forests 9, 145. https://doi.org/10.3390/f9030145.

De Ridder, K., 2010. Bulk transfer relations for the roughness sublayer. Bound.-Layer Meteorol. 134, 257–267. https://doi.org/10.1007/s10546-009-9450-y.

Devaraju, N., de Noblet-Ducoudré, N., Quesada, B., Bala, G., 2018. Quantifying the relative importance of direct and indirect biophysical effects of deforestation on surface temperature and teleconnections. J. Climate 31, 3811–3829. https://doi.org/10.1175/JCLI-D-17-0563.1.

Euskirchen, E.S., Bret-Harte, M.S., Shaver, G.R., Edgar, C.W., Romanovsky, V.E., 2017. Long-Term release of carbon dioxide from arctic tundra ecosystems in Alaska. Ecosystems 20, 960–974. https://doi.org/10.1007/s10021-016-0085-9.

Fitzjarrald, D.R., Acevedo, O.C., Moore, K.E., 2001. Climatic consequences of leaf presence in the eastern united states. J. Climate 14, 598–614. https://doi.org/10.1175/1520-0442(2001)014<0598:CCOLPI>2.0.CO;2.

Foken, T., 2008. THE energy balance closure PROBLEM: an overview. Ecol. Appl. 18, 1351–1367. https://doi.org/10.1890/06-0922.1.

Frank, J.M., Massman, W.J., Ewers, B.E., Huckaby, L.S., Negrón, J.F., 2014. Ecosystem CO2/H2O fluxes are explained by hydraulically limited gas exchange during tree mortality from spruce bark beetles. J. Geophys. Res. 119, 1195–1215. https://doi.org/10.1002/2013JG002597.

Freedman, J.M., Fitzjarrald, D.R., Moore, K.E., Sakai, R.K., 2001. Boundary layer clouds and Vegetation–Atmosphere feedbacks. J. Climate 14, 180–197. https://doi.org/10.1175/1520-0442(2001)013<0180:BLCAVA>2.0.CO;2.

Friedl, M.A., Gray, J.M., Melaas, E.K., Richardson, A.D., Hufkens, K., Keenan, T.F., Bailey, Amey, O'Keefe, J., 2014. A tale of two springs: using recent climate anomalies to characterize the sensitivity of temperate forest phenology to climate change. Environ. Res. Lett. 9, 054006. https://doi.org/10.1088/1748-9326/9/5/054006.

Ganguly, S., Friedl, M.A., Tan, B., Zhang, X., Verma, M., 2010. Land surface phenology from MODIS: characterization of the collection 5 global land cover dynamics product. Remote Sens. Environ. 114, 1805–1816. https://doi.org/10.1016/j.rse.2010.04.005.

Garratt, J.R., 1992. The Atmospheric Boundary Layer. Cambridge University Press, New York.

Gentine, P., Chhang, A., Rigden, A., Salvucci, G., 2016. Evaporation estimates using weather station data and boundary layer theory. Geophys. Res. Lett. 43https://doi.org/10.1002/2016GL070819. 11,661-11,670.

Gilmanov, T.G., Tieszen, L.L., Wylie, B.K., Flanagan, L.B., Frank, A.B., Haferkamp, M.R.,

Meyers, T.P., Morgan, J.A., 2005. Integration of CO2 flux and remotely-sensed data for primary production and ecosystem respiration analyses in the Northern Great Plains: potential for quantitative spatial extrapolation. Glob. Ecol. Biogeogr. 14, 271–292. https://doi.org/10.1111/j.1466-822X.2005.00151.x.

Gough, C.M., Hardiman, B.S., Nave, L.E., Bohrer, G., Maurer, K.D., Vogel, C.S., Nadelhoffer, K.J., Curtis, P.S., 2013. Sustained carbon uptake and storage following moderate disturbance in a Great Lakes forest. Ecol. Appl. 23, 1202–1215. https://doi.org/10.1890/12-1554.1.

Gu, L., Hanson, P.J., Post, W.M., Kaiser, D.P., Yang, B., Nemani, R., Pallardy, S.G., Meyers, T., 2008. The 2007 eastern us spring freeze: increased cold damage in a warming world? Bioscience 58, 253–262. https://doi.org/10.1641/B580311.

Harman, I.N., Finnigan, J.J., 2007. A simple unified theory for flow in the canopy and roughness sublayer. Bound.-Layer Meteorol. 123, 339–363. https://doi.org/10.1007/s10546-006-9145-6.

Heerwaarden, C.C., Arellano, J.V.-G., Moene, A.F., Holtslag, A.A.M., 2009. Interactions between dry-air entrainment, surface evaporation and convective boundary-layer development. Q. J. R. Meteorol. Soc. 135, 1277–1291. https://doi.org/10.1002/qj.431.

Hemes, K.S., Chamberlain, S.D., Eichelmann, E., Anthony, T., Valach, A., Kasak, K., Szutu, D., Verfaillie, J., Silver, W.L., Baldocchi, D.D., 2019. Assessing the carbon and climate benefit of restoring degraded agricultural peat soils to managed wetlands. Agric. Forest Meteorol. 268, 202–214. https://doi.org/10.1016/j.agrformet.2019.01.017.

Hiller, R.V., McFadden, J.P., Kljun, N., 2011. Interpreting CO2 fluxes over a suburban lawn: the influence of traffic emissions. Bound.-Layer Meteorol. 138, 215–230. https://doi.org/10.1007/s10546-010-9558-0.

Hogg, E.H., Price, D.T., Black, T.A., 2000. Postulated feedbacks of deciduous forest phenology on seasonal climate patterns in the Western Canadian interior. J. Climate 13, 4229–4243. https://doi.org/10.1175/1520-0442(2000)013<4229:PFODFP>2.0.CO;2.

Hollinger, D.Y., Aber, J., Dail, B., Davidson, E.A., Goltz, S.M., Hughes, H., Leclerc, M.Y., Lee, J.T., Richardson, A.D., Rodrigues, C., Scott, N.A., Achuatavarier, D., Walsh, J., 2004. Spatial and temporal variability in forest–atmosphere CO2 exchange. Glob. Chang Biol. 10, 1689–1706. https://doi.org/10.1111/j.1365-2486.2004.00847.x.

Jacobs, C.M.J., De Bruin, H., 1992. The sensitivity of regional transpiration to land-surface characteristics: significance of feedback. J. Climate 5, 683–698. https://doi.org/10.1175/1520-0442(1992)005<0683:TSORTT>2.0.CO;2.

Jarvis, P.G., McNaughton, K.G., 1986. Stomatal control of transpiration: scaling up from leaf to region. In: MacFadyen, A., Ford, E.D. (Eds.), Advances in Ecological Research. Academic Press, pp. 1–49. https://doi.org/10.1016/S0065-2504(08)60119-1.

Jarvis, P.G., Monteith, J.L., Weatherley, P.E., 1976. The interpretation of the variations in leaf water potential and stomatal conductance found in canopies in the field. Philos. Trans. R. Soc. Lond. B, Biol. Sci. 273, 593–610. https://doi.org/10.1098/rstb.1976.0035.

Juang, J.-Y., Katul, G.G., Porporato, A., Stoy, P.C., Siqueira, M.S., Detto, M., Kim, H.-S., Oren, R., 2007. Eco-hydrological controls on summertime convective rainfall triggers. Glob. Chang Biol. 13, 887–896. https://doi.org/10.1111/j.1365-2486.2007.01315.x.

Kwon, H., Law, B.E., Thomas, C.K., Johnson, B.G., 2018. The influence of hydrological variability on inherent water use efficiency in forests of contrasting composition, age, and precipitation regimes in the Pacific Northwest. Agric. Forest Meteorol. 249, 488–500. https://doi.org/10.1016/j.agrformet.2017.08.006.

Lee, X., Goulden, M.L., Hollinger, D.Y., Barr, A., Black, T.A., Bohrer, G., Bracho, R., Drake, B., Goldstein, A., Gu, L., Katul, G., Kolb, T., Law, B.E., Margolis, H., Meyers, T., Monson, R., Munger, W., Oren, R., U, K.T.P., Richardson, A.D., Schmid, H.P., Staebler, R., Wofsy, S., Zhao, L., 2011. Observed increase in local cooling effect of deforestation at higher latitudes. Nature 479, 384–387. https://doi.org/10.1038/nature10588.

Li, D., Liao, W., Rigden, A.J., Liu, X., Wang, D., Malyshev, S., Shevliakova, E., 2019. Urban heat island: aerodynamics or imperviousness? Sci. Adv. 5https://doi.org/10.1126/sciadv.aau4299. eaau4299.

Li, D., Wang, L., 2019. Sensitivity of surface temperature to land use and land cover change-induced biophysical changes: the scale issue. Geophys. Res. Lett. 46, 9678–9689. https://doi.org/10.1029/2019GL084861.

Liao, W., Rigden, A.J., Li, D., 2018. Attribution of local temperature response to deforestation. J. Geophys. Res. https://doi.org/10.1029/2018JG004401. 0.

Luyssaert, S., Jammet, M., Stoy, P.C., Estel, S., Pongratz, J., Ceschia, E., Churkina, G., Don, A., Erb, K., Ferlicoq, M., Gielen, B., Grünwald, T., Houghton, R.A., Klumpp, K., Knohl, A., Kolb, T., Kuemmerle, T., Laurila, T., Lohila, A., Loustau, D., McGrath, M.J., Meyfroidt, P., Moors, E.J., Naudts, K., Novick, K., Otto, J., Pilegaard, K., Pio, C.A., Rambal, S., Rebmann, C., Ryder, J., Suyker, A.E., Varlagin, A., Wattenbach, M., Dolman, A.J., 2014. Land management and land-cover change have impacts of similar magnitude on surface temperature. Nat. Clim. Chang 4, 389–393. https://doi.org/10.1038/nclimate2196.

McCaughey, J.H., Pejam, M.R., Arain, M.A., Cameron, D.A., 2006. Carbon dioxide and energy fluxes from a boreal mixedwood forest ecosystem in Ontario, Canada. Agric. Forest Meteorol. Fluxnet-Canada Res. Netw. 140, 79–96. https://doi.org/10.1016/j.agrformet.2006.08.010.

McNaughton, K.G., Spriggs, T.W., 1986. A mixed-layer model for regional evaporation. Bound.-Layer Meteorol. 34, 243–262. https://doi.org/10.1007/BF00122381.

Meyers, T.P., Hollinger, S.E., 2004. An assessment of storage terms in the surface energy balance of maize and soybean. Agric. Forest Meteorol. 125, 105–115. https://doi.org/10.1016/j.agrformet.2004.03.001.

Monteith, J.L., Unsworth, M.H., 2013. Principles of Environmental Physics: Plants, Animals, and the Atmosphere, 4th ed. Elsevier/Academic Press, Amsterdam; Boston.

Moon, M., Zhang, X., Henebry, G.M., Liu, L., Gray, J.M., Melaas, E.K., Friedl, M.A., 2019. Long-term continuity in land surface phenology measurements: a comparative assessment of the MODIS land cover dynamics and VIIRS land surface phenology products. Remote Sens. Environ. 226, 74–92. https://doi.org/10.1016/j.rse.2019.03.034.

Moore, K.E., Fitzjarrald, D.R., Sakai, R.K., Goulden, M.L., Munger, J.W., Wofsy, S.C., 1996. Seasonal variation in radiative and turbulent exchange at a deciduous forest in central Massachusetts. J. Appl. Meteor. 35, 122–134. https://doi.org/10.1175/1520-0450(1996)035<0122:SVIRAT>2.0.CO;2.

Noormets, A., Gavazzi, M.J., Mcnulty, S.G., Domec, J.-C., Sun, G., King, J.S., Chen, J., 2010. Response of carbon fluxes to drought in a coastal plain loblolly pine forest. Glob. Chang Biol. 16, 272–287. https://doi.org/10.1111/j.1365-2486.2009.01928.x.

Noormets, A., McNulty, S.G., Domec, J.-C., Gavazzi, M., Sun, G., King, J.S., 2012. The role of harvest residue in rotation cycle carbon balance in loblolly pine plantations. Respiration partitioning approach. Glob. Change Biol. 18, 3186–3201. https://doi.org/10.1111/j.1365-2486.2012.02776.x.

Oishi, A.C., Oren, R., Stoy, P.C., 2008. Estimating components of forest evapotranspiration: a footprint approach for scaling sap flux measurements. Agric. Forest Meteorol. 148, 1719–1732. https://doi.org/10.1016/j.agrformet.2008.06.013.

Ollinger, S.V., Richardson, A.D., Martin, M.E., Hollinger, D.Y., Frolking, S.E., Reich, P.B., Plourde, L.C., Katul, G.G., Munger, J.W., Oren, R., Smith, M.-L., U, K.T.P., Bolstad, P.V., Cook, B.D., Day, M.C., Martin, T.A., Monson, R.K., Schmid, H.P., 2008. Canopy nitrogen, carbon assimilation, and albedo in temperate and boreal forests: functional relations and potential climate feedbacks. PNAS 105, 19336–19341. https://doi.org/10.1073/pnas.0810021105.

Oren, R., Hsieh, C.-I., Stoy, P., Albertson, J., Mccarthy, H.R., Harrell, P., Katul, G.G., 2006. Estimating the uncertainty in annual net ecosystem carbon exchange: spatial variation in turbulent fluxes and sampling errors in eddy-covariance measurements. Glob. Chang Biol. 12, 883–896. https://doi.org/10.1111/j.1365-2486.2006.01131.x.

Parker, G.G., Russ, M.E., 2004. The canopy surface and stand development: assessing forest canopy structure and complexity with near-surface altimetry. Forest Ecol. Manage. 189, 307–315. https://doi.org/10.1016/j.foreco.2003.09.001.

Peichl, M., Arain, M.A., Brodeur, J.J., 2010. Age effects on carbon fluxes in temperate pine forests. Agric. Forest Meteorol. 150, 1090–1101. https://doi.org/10.1016/j.agrformet.2010.04.008.

Peñuelas, J., Rutishauser, T., Filella, I., 2009. Phenology feedbacks on climate change. Science 324, 887–888. https://doi.org/10.1126/science.1173004.

Pielke Sr., R.A., Avissar, R., Raupach, M., Dolman, A.J., Zeng, X., Denning, A.S., 1998. Interactions between the atmosphere and terrestrial ecosystems: influence on weather and climate. Glob. Chang Biol. 4, 461–475. https://doi.org/10.1046/j.1365-2486.1998.t01-1-00176.x.

Richardson, A.D., Hufkens, K., Milliman, T., Frolking, S., 2018. Intercomparison of phenological transition dates derived from the Phenocam dataset V1.0 and MODIS satellite remote sensing. Sci. Rep. 8, 5679. https://doi.org/10.1038/s41598-018-23804-6.

Richardson, A.D., Keenan, T.F., Migliavacca, M., Ryu, Y., Sonnentag, O., Toomey, M., 2013. Climate change, phenology, and phenological control of vegetation feedbacks to the climate system. Agric. Forest Meteorol. 169, 156–173. https://doi.org/10.1016/j.agrformet.2012.09.012.

Rienecker, M.M., Suarez, M.J., Gelaro, R., Todling, R., Bacmeister, J., Liu, E., Bosilovich, M.G., Schubert, S.D., Takacs, L., Kim, G.-K., Bloom, S., Chen, J., Collins, D., Conaty, A., da Silva, A., Gu, W., Joiner, J., Koster, R.D., Lucchesi, R., Molod, A., Owens, T., Pawson, S., Pegion, P., Redder, C.R., Reichle, R., Robertson, F.R., Ruddick, A.G., Sienkiewicz, M., Woollen, J., 2011. MERRA: NASA's Modern-Era retrospective analysis for research and applications. J. Climate 24, 3624–3648. https://doi.org/10.1175/JCLI-D-11-00015.1.

Rigden, A., Li, D., Salvucci, G., 2018. Dependence of thermal roughness length on friction velocity across land cover types: a synthesis analysis using ameriflux data. Agric. Forest Meteorol. 249, 512–519. https://doi.org/10.1016/j.agrformet.2017.06.003.

Rigden, A.J., Li, D., 2017. Attribution of surface temperature anomalies induced by land use and land cover changes. Geophys. Res. Lett. 44, 6814–6822. https://doi.org/10.1002/2017GL073811.

Runkle, B.R.K., Rigby, J.R., Reba, M.L., Anapalli, S.S., Bhattacharjee, J., Krauss, K.W., Liang, L., Locke, M.A., Novick, K.A., Sui, R., Suvočarev, K., White, P.M., 2017. DeltaFlux: an eddy covariance network for a climate-smart lower Mississippi Basin. Agric. Environ. Lett. 2. https://doi.org/10.2134/ael2017.01.0003.

Ryu, Y., Baldocchi, D.D., Ma, S., Hehn, T., 2008. Interannual variability of evapotranspiration and energy exchange over an annual grassland in California. J. Geophys. Res. 113. https://doi.org/10.1029/2007JD009263.

Sakai, R.K., Fitzjarrald, D.R., Moore, K.E., 1997. Detecting leaf area and surface resistance during transition seasons. Agric. Forest Meteorol. 84, 273–284. https://doi.org/10.1016/S0168-1923(96)02359-3.

Santanello, J.A., Dirmeyer, P.A., Ferguson, C.R., Findell, K.L., Tawfik, A.B., Berg, A., Ek, M., Gentine, P., Guillod, B.P., van Heerwaarden, C., Roundy, J., Wulfmeyer, V., 2018. Land–Atmosphere interactions: the loco perspective. Bull. Amer. Meteor. Soc. 99, 1253–1272. https://doi.org/10.1175/BAMS-D-17-0001.1.

Schwartz, M.D., 1996. Examining the spring discontinuity in daily temperature ranges. J. Climate 9, 803–808. https://doi.org/10.1175/1520-0442(1996)009<0803:ETSDID>2.0.CO;2.

Schwartz, M.D., 1992. Phenology and springtime surface-layer change. Mon. Wea. Rev. 120, 2570–2578. https://doi.org/10.1175/1520-0493(1992)120<2570:PASSLC>2.0.CO;2.

Schwartz, M.D., Crawford, T.M., 2001. Detecting energy-balance modifications at the onset of spring. Phys. Geogr. 22, 394–409. https://doi.org/10.1080/02723646.2001.10642751.

Sellers, P.J., Dickinson, R.E., Randall, D.A., Betts, A.K., Hall, F.G., Berry, J.A., Collatz, G.J., Denning, A.S., Mooney, H.A., Nobre, C.A., Sato, N., Field, C.B., Henderson-Sellers, A., 1997. Modeling the exchanges of energy, water, and carbon between

continents and the atmosphere. Science 275, 502–509. https://doi.org/10.1126/science.275.5299.502.
Shaw, R.H., Pereira, A.R., 1982. Aerodynamic roughness of a plant canopy: a numerical experiment. Agric. Meteorol. 26, 51–65. https://doi.org/10.1016/0002-1571(82)90057-7.
Stewart, J.B., 1988. Modelling surface conductance of pine forest. Agric. Forest Meteorol. 43, 19–35. https://doi.org/10.1016/0168-1923(88)90003-2.
Suyker, A.E., Verma, S.B., Burba, G.G., Arkebauer, T.J., 2005. Gross primary production and ecosystem respiration of irrigated maize and irrigated soybean during a growing season. Agric. Forest Meteorol. 131, 180–190. https://doi.org/10.1016/j.agrformet.2005.05.007.
Thornton, P.E., Law, B.E., Gholz, H.L., Clark, K.L., Falge, E., Ellsworth, D.S., Goldstein, A.H., Monson, R.K., Hollinger, D., Falk, M., Chen, J., Sparks, J.P., 2002. Modeling and measuring the effects of disturbance history and climate on carbon and water budgets in evergreen needleleaf forests. Agric. Forest Meteorol., FLUXNET 2000 Synthesis 113, 185–222. https://doi.org/10.1016/S0168-1923(02)00108-9.
van Heerwaarden, C.C., Vilà-Guerau de Arellano, J., Gounou, A., Guichard, F., Couvreux, F., 2010. Understanding the daily cycle of evapotranspiration: a method to quantify the influence of forcings and feedbacks. J. Hydrometeor. 11, 1405–1422. https://doi.org/10.1175/2010JHM1272.1.
Wang, P., Li, D., Liao, W., Rigden, A., Wang, W., 2019. Contrasting evaporative responses of ecosystems to heatwaves traced to the opposing roles of vapor pressure deficit and surface resistance. Water Resour. Res. https://doi.org/10.1029/2019WR024771. 0.
Wang, Z., Schaaf, C.B., Sun, Q., Shuai, Y., Román, M.O., 2018. Capturing rapid land surface dynamics with collection V006 MODIS BRDF/NBAR/Albedo (MCD43) products. Remote Sens. Environ. 207, 50–64. https://doi.org/10.1016/j.rse.2018.02.001.
Wilson, K.B., Baldocchi, D.D., 2000. Seasonal and interannual variability of energy fluxes over a broadleaved temperate deciduous forest in North America. Agric. Forest Meteorol. 100, 1–18. https://doi.org/10.1016/S0168-1923(99)00088-X.
Wolf, S., Keenan, T.F., Fisher, J.B., Baldocchi, D.D., Desai, A.R., Richardson, A.D., Scott, R.L., Law, B.E., Litvak, M.E., Brunsell, N.A., Peters, W., van der Laan-Luijkx, I.T., 2016. Warm spring reduced carbon cycle impact of the 2012 US summer drought. Proc. Natl. Acad. Sci. 113, 5880–5885. https://doi.org/10.1073/pnas.1519620113.
Wood, J.D., Sadler, E.J., Fox, N.I., Greer, S.T., Gu, L., Guinan, P.E., Lupo, A.R., Market, P.S., Rochette, S.M., Speck, A., White, L.D., 2019. Land-Atmosphere responses to a total solar eclipse in three ecosystems with contrasting structure and physiology. J. Geophys. Res. 124, 530–543. https://doi.org/10.1029/2018JD029630.
Wouters, H., Petrova, I.Y., van Heerwaarden, C.C., Vilà-Guerau de Arellano, J., Teuling, A.J., Meulenberg, V., Santanello, J.A., Miralles, D.G., 2019. Atmospheric boundary layer dynamics from balloon soundings worldwide: CLASS4GL v1.0. Geosci. Model Dev. 12, 2139–2153. https://doi.org/10.5194/gmd-12-2139-2019.
Xiao, X., Hollinger, D., Aber, J., Goltz, M., Davidson, E.A., Zhang, Q., Moore, B., 2004. Satellite-based modeling of gross primary production in an evergreen needleleaf forest. Remote Sens. Environ. 89, 519–534. https://doi.org/10.1016/j.rse.2003.11.008.
Zeller, K., 2000. Wintertime ozone fluxes and profiles above a subalpine spruce–fir forest. J. Appl. Meteor. 39, 92–101. https://doi.org/10.1175/1520-0450(2000)039<0092:WOFAPA>2.0.CO;2.
Zhang, Q., Phillips, R.P., Manzoni, S., Scott, R.L., Oishi, A.C., Finzi, A., Daly, E., Vargas, R., Novick, K.A., 2018. Changes in photosynthesis and soil moisture drive the seasonal soil respiration-temperature hysteresis relationship. Agric. Forest Meteorol. 259, 184–195. https://doi.org/10.1016/j.agrformet.2018.05.005.
Zhang, X., Friedl, M.A., Schaaf, C.B., Strahler, A.H., Liu, Z., 2005. Monitoring the response of vegetation phenology to precipitation in Africa by coupling MODIS and TRMM instruments. J. Geophys. Res. 110. https://doi.org/10.1029/2004JD005263.
Zhang, Y., Li, D., Lin, Z., Santanello, J.A., Gao, Z., 2019. Development and evaluation of a long-term data record of planetary boundary layer profiles from aircraft meteorological reports. J. Geophys. Res. 124, 2008–2030. https://doi.org/10.1029/2018JD029529.
Zhao, L., Lee, X., Smith, R.B., Oleson, K., 2014. Strong contributions of local background climate to urban heat islands. Nature 511, 216–219. https://doi.org/10.1038/nature13462.
Zhao, L., Lee, X., Suyker, A.E., Wen, X., 2016. Influence of leaf area index on the radiometric resistance to heat transfer. Bound.-Layer Meteorol. 158, 105–123. https://doi.org/10.1007/s10546-015-0070-4.